Chaotic Einstein-Podolsky-Rosen pairs, measurements and time reversal

Klaus M. Frahm and Dima L. Shepelyansky

Laboratoire de Physique Théorique, Université de Toulouse, CNRS, UPS, 31062 Toulouse, France

(Dated: June 6, 2021)

Abstract: We consider a situation when evolution of an entangled Einstein-Podolsky-Rosen (EPR) pair takes place in a regime of quantum chaos being chaotic in the classical limit. This situation is studied on an example of chaotic pair dynamics described by the quantum Chirikov standard map. The time evolution is reversible even if a presence of small errors breaks time reversal of classical dynamics due to exponential growth of errors induced by exponential chaos instability. However, the quantum evolution remains reversible since a quantum dynamics instability exists only on a logarithmically short Ehrenfest time scale. We show that due to EPR pair entanglement a measurement of one particle at the moment of time reversal breaks exact time reversal of another particle which demonstrates only an approximate time reversibility. This result is interpreted in the framework of the Schmidt decomposition and Feynman path integral formulation of quantum mechanics. The time reversal in this system has already been realized with cold atoms in kicked optical lattices in absence of entanglement and measurements. On the basis of the obtained results we argue that the experimental investigations of time reversal of chaotic EPR pairs is within reach of present cold atom capabilities.

I. INTRODUCTION

The fundamental work of Einstein-Podolsky-Rosen (EPR) [1] on a distant entanglement of a pair of non-interacting distinguished particles and its effects on measurements is now at the foundations of long-distance quantum communications. The entanglement concept coined by Schrödinger [2] with a gedanken experiment of a cat, dead or alive, becomes a resource of modern quantum computations [3, 4]. An impressive modern progress of quantum information, computation and communication is described in [5].

An overview of various experimental realizations of EPR pairs is given in [6]. Various forms of propagating EPR pairs have been studied experimentally but in its main aspect the propagation of EPR pairs was rather simple being similar to propagation on a line and always being integrable. Here we consider theoretically a situation when two non-interacting but entangled particles of an EPR pair propagate in a regime of quantum chaos [7]. In the classical limit a dynamics of these particles is chaotic being characterized by an exponential local divergence of trajectories with a positive Kolmogorov-Sinai entropy h [8–11]. The exponential instability of chaotic dynamics leads to exponential growth of round-off errors and breaking of time reversibility of classical evolution described by reversible equations of motion. Thus chaos resolves the famous Loschmidt-Boltzmann dispute on time reversibility and emergence of statistical laws from reversible dynamical equations [12–14] (see also [15]). Prior to classical chaos theory the problem of time reversal of laws of nature was also discussed by such leading scientists as Schrödinger [16] (see English translation and overview in [17]) and Kolmogorov [18].

However, in quantum mechanics a chaotic mixing in a phase-space cannot go down to exponentially small scales being restricted by a quantum scale of the Planck constant $\hbar$. Thus in the regime of quantum chaos an exponential instability exists only during a logarithmically short Ehrenfest time scale $\tau_E \sim |\ln \hbar|/h$ [19–22] (here $\hbar$ is a dimensionless effective Planck constant related to typical quantum numbers). Due to the absence of exponential instability on times beyond τ_E the quantum evolution remains reversible in presence of quantum errors in a drastic difference from the classical dynamics as it was demonstrated in [23] for the quantum Chirikov standard map, also known as a kicked rotator [19, 21, 24]. This system has been experimentally realized with cold atoms in kicked optical lattices and in particular the quantum dynamical localization of chaotic diffusion has been observed in these experiments [25, 26]. This dynamical localization of chaotic diffusion appears due to quantum interference and is analogous to the Anderson localization [27] of electron diffusion in disordered solids (see e.g. [28–30]).

In [31] it was shown that the time evolution of cold atoms in kicked optical lattices, described by the quantum Chirikov standard map, can be reversed in time in the regime of quantum chaos. This proposal was indeed experimentally realized by the Hoogerland group [32]. Thus this system represents an efficient experimental platform which allows to investigate nontrivial effects of quantum mechanics, localization, chaos and time reversal.

In this work we investigate the properties of chaotic EPR pairs evolving in this fundamental system of quantum chaos and show that a measurement of one of the entangled particles breaks exact time reversal of the other particle but preserves its approximate time reversibility. We explain this unusual effect on the basis of the Schmidt decomposition [33] (see also the review [34] and Refs. therein) and the Feynman path integral formulation of quantum mechanics [35].

This article is composed as follows: the model is described in Section II, the results are presented in Section III and the discussion and conclusion are given in Section IV; additional Figures and data are given in Appendix.

II. MODEL DESCRIPTION

The classical dynamics of one particle is described by the Chirikov standard map [10]:

$$\bar{p} = p + k \sin x , \quad \bar{x} = x + T\bar{p} . \tag{1}$$

Here x represents the position of an atom in an infinite $x-$axis of the kicked optical lattice, or a cyclic variable $0 \leq x < 2\pi$ for the case of the kicked rotator; p is the momentum of a particle. The bars denote the new values of variables after one iteration of this symplectic map. The physical process described by this map corresponds to a sharp change of momentum, generated e.g. by a kick of the optical lattice [25, 26], followed by a free particle propagation during a period T between kicks. The classical dynamics depends on a single chaos parameter $K = kT$ with a transition from integrability to unlimited chaotic diffusion in momentum for $K > K_c = 0.9715...$ [10, 11]. The system dynamics is reversible in time, e.g. by inverting all velocities in a middle of free rotation between two kicks.

Inside a chaotic component the dynamics is characterized by an exponential divergence of trajectories with the positive Kolmogorov-Sinai entropy h. For $K > 4$ the measure of stability islands is small and we have $h \approx \ln(K/2)$ [10]. For $K > K_c$ the dispersion of momentum grows diffusively with time $\langle (\Delta p)^2 \rangle = Dt$ with a diffusion coefficient $D \approx k^2/2$ (see more details in [10, 30]). Here and below the time t is measured in number of map iterations. The map captures a variety of universal features of dynamical chaos and appears in the description of various physical systems [24].

The quantum evolution of the state $|\psi\rangle$ over a period is given by a unitary operator $\hat{U}$ [19, 21]:

$$|\bar{\psi}\rangle = \hat{U}|\psi\rangle = e^{-iT\hat{p}^2/2} e^{-ik\cos \hat{x}} |\psi\rangle . \tag{2}$$

Here the momentum p is measured in recoil units of optical lattice with $\hat{p} = -i\partial/\partial x$. Thus $T = \hbar$ plays the role of an effective dimensionless Planck constant and the classical limit corresponds to $T = \hbar \to 0$, $k \to \infty$, $K = kT = const$. Due to the periodicity of the optical lattice potential the momentum operator $\hat{p} = -i\partial/\partial x$ has eigenvalues $p = n+\beta$ where n is an integer and β is a quasimomentum conserved by the kick potential ($0 \leq \beta < 1$). The value $\beta = 0$ corresponds to the case of a kicked rotator with a wave function (in position representation) $\psi(x) = \langle x|\psi\rangle$ being periodic on a circle $\psi(x + 2\pi) = \psi(x)$. In this case the free rotation correspond (in momentum representation) to the phase shift $\bar{\psi}_{n,0} = \exp(-iTn^2/2)\psi_{n,0}$

with $\psi_{n,\beta} = \langle p|\psi\rangle$ being the wave function (in momentum representation) at $p = n + \beta$. Irrational values of β appear for a particle propagation on an infinite x-axis; here β is conserved and a free propagation of the momentum wave function $\psi_{n,\beta}$ gives the phase shift $\bar{\psi}_{n,\beta} = \exp(-iT(n+\beta)^2/2)\psi_{n,\beta}$. The effects of quantum interference lead to dynamical localization of chaotic diffusion on a time scale $t_D \approx D/\hbar^2 \gg \tau_E$ and an exponential localization of quasienergy eigenstates with a localization length $\ell = D/(2\hbar^2) \approx k^2/4$ [21, 30].

In [31] it was pointed that the time reversal of a quantum evolution after t_r map iterations can be realized by using a period between kicks being $T = 4\pi + \epsilon$ for $t \leq t_r$ and $T' = 4\pi - \epsilon$ for $t_r < t \leq 2t_r$. Also the time reversal is done at the middle of the free propagation after t_r kicks (it is convenient to use a symmetrized scheme with a half-period of free rotation then kick and then again a half-period of free propagation). The inversion of kick amplitude $k\cos x \to -k\cos x$ can be realized by a π-translational shift of the optical lattice potential. Such a time reversal is exact for $\beta = 0$ (kicked rotator case) and it also works approximately for small β values in the case of the kicked particle [31]. The time reversal for cold atoms in a kicked optical lattice was experimentally demonstrated in [32].

Here we consider the time reversal of two non-interacting distinguished particles being in an initial entangled state. We concentrate our analysis on the case when both particles evolve in the regime of quantum chaos. Thus we have the new case of chaotic EPR pairs. Following (2) the evolution of the two particle state $|\psi\rangle$ (with wave function $\psi(x_1, x_2) = \langle x_1, x_2|\psi\rangle$) of such pairs is given by the quantum map

$$|\bar{\psi}\rangle = (\hat{U}_1 \otimes \hat{U}_2)|\psi\rangle , \tag{3}$$

where $\hat{U}_1$ and $\hat{U}_2$ are one time period evolution operators for the first and second particle. In absence of interactions between particles the entropy of entanglement S is preserved during this time evolution. It is convenient to use the Schmidt decomposition [33, 34] for an initial entangled state

$$|\psi\rangle = \sum_{i=1}^{m} \alpha_i |u_i\rangle \otimes |v_i\rangle \tag{4}$$

where $|u_i\rangle$, $|v_i\rangle$ are one-particle states satisfying the orthogonality relations: $\langle u_i|u_j\rangle = \langle v_i|v_j\rangle = \delta_{ij}$. The number m of Schmidt components can be up to $m = N$ if N is the dimension of the one-particle Hilbert space. However, for "less" entangled states m may be smaller and in this work we will consider the case of $m = 2$. The entropy of entanglement is then given by (see e.g. [3, 34]):

$$S = -Tr(\rho_1 \log_2 \rho_1) = -\sum_i |\alpha_i|^2 \log_2 |\alpha_i|^2 , \tag{5}$$

where ρ_1 is a reduced density matrix of first particle obtained by a trace taken over the second particle. During the time evolution of EPR pair given by (3) the wave functions of each particle evolve independently with $|u_i(t)\rangle = \hat{U}_1^t|u_i(t=0)\rangle$ and $|v_i(t)\rangle = \hat{U}_1^t|v_i(t=0)\rangle$. Thus the coefficients α_i of the Schmidt decomposition and the entropy of entanglement S remain unchanged.

However, since the particles are entangled a measurement of the second particle after the time t_r affects the wave function of first particle and thus the time reversal evolution of this particle is modified so that the exact time reversibility is broken by the measurement. Nevertheless, we will see that still there is an approximate time reversal of the first particle. We describe in detail this effect in the next section.

III. TIME EVOLUTION OF CHAOTIC EPR PAIRS

The numerical simulations of the quantum map (2), (3) are done in a usual way [19, 21] by using the fact that the free propagation and the kick are diagonal in the momentum and coordinate representations respectively. Concerning the eigenphases $Tn^2/2$ of the free propagation operator we mention an important technical detail: we compute these phases for $n = -N/2, \ldots, N/2 - 1$ (with N being the dimension of the one-particle Hilbert space) and the values for $n < 0$ are stored at the positions $N - n$ while the values for $n \geq 0$ are stored at positions n. In this way if the initial states are localized close to small values of $n \approx 0$ (or $n \approx N$ which is topologically close to $n \approx 0$ due to the periodic boundary conditions) and if during the time evolution the states do not touch the borders at $n \approx \pm N/2$ the results are independent of the exact choice N provided N is sufficiently large. In other words the momentum phases exhibit a smooth transition between $n \approx 0$ and $n \approx N$ according the quadratic formula while at the "system border" $n \approx N/2$ this transition is not smooth. Otherwise, if the phases were naively computed for $n = 0, \ldots, N-1$ according to the quadratic formula the results would depend in a sensitive way on N even if the states remain localized close to $n \approx 0$ since the eigenphases for $n \approx N$ would be very different.

The transitions from one representation (momentum or position) to another and back are done with the Fast Fourier Transform (FFT). Furthermore, we chose the quantum map to be directly symmetric in time and therefore we present it as a half period of free propagation (using the operator $\hat{U}_{\text{half,free}} = e^{-iT\hat{p}^2/4}$) followed by the kick (using $\hat{U}_{\text{kick}} = e^{-ik\cos\hat{x}}$) and then again a half period of free propagation (using $\hat{U}_{\text{half,free}}$). Furthermore, in order to have an exact mathematical equivalence between the two cases $T = 4\pi + \epsilon$ and $T = \epsilon$ (at $\beta = 0$) we also apply for the first case to the initial states (given below

for the different cases we consider) an initial half period of free propagation with $T = 4\pi$ (which provides an additional phase factor $(-1)^{n_1+n_2}$ in momentum representation). We have numerically verified that this equivalence is indeed valid.

We consider in detail 3 specific cases: A) kicked rotator case with a moderate dimensionless effective Planck constant $\hbar_{\text{eff}} = \epsilon = T - 4\pi < 1$ and a wavefunction periodic on the 2π-circle (i.e. integer values of $p_i = n_i$ with $\beta_i = 0$ and $i = 1, 2$ for both particles); B) same case but taken in the deep semiclassical regime with $\hbar_{\text{eff}} \ll 1$; C) the case of kicked particles propagation on an infinite (or quasi-infinite) line at moderate $\hbar_{\text{eff}}$ that corresponds to the case of cold atoms in a kicked optical lattice [25, 26, 32] composed of L periods such that $x \in [0, 2\pi L$. The total computational basis size for one particle, used in the numerical simulations, was changing from $N = 1024$ up to $N = 2^{22}$, depending on the choice of A), B), C) and insuring that the basis size does not affect the obtained results. For two particles the size of the Hilbert space is $N_H = N^2$. For moderate values of N (e.g. up to $N = 2^{12}$ in cases A and B) we used the whole basis with N_H states using two-dimensional (2D) FFT transitions between momentum and coordinate representations in (3). For larger N values we used the fact that the Schmidt decomposition (4) has coefficients α_i being unchanged during the time evolution so that we propagate independently each particle and use the Schmidt entangled EPR wavefunction for a measurement of the second particle at the time moment t_r and backward propagating only the first particle after measurement. We checked, for $N \leq 2^{12}$, that these two numerical methods of time evolution simulation give the same results up to the computer numerical accuracy. Some additional details about numerical simulations and Figures are given in the Appendix.

IIIA. EPR pairs in kicked rotator at moderate $\hbar_{\text{eff}}$ values

Here we present the results for a case with moderate effective value of the Planck constant. As described above we use the values of parameter $T = 4\pi + \epsilon$ for forward time propagation with t_r quantum map iterations and $T = 4\pi - \epsilon$ for next t_r iterations corresponding to the time reversal. We remind that since the phase shift $(4\pi)n^2/2$ is a multiple of 2π for all integer values of the momentum $p = n$ the evolution is determined by an effective Planck constant $\hbar_{\text{eff}} = \epsilon$. Thus the effective classical chaos parameter is $K_{\text{eff}} = k\epsilon = k\hbar_{\text{eff}}$. The measurement is done for the second particle after t_r iterations. We consider the case of projective measurement in the momentum basis n_2 of the second particle performing the projection to a certain value of n_2 after t_r iterations. After that the evolution of the first particle continues with $T = 4\pi - \epsilon$ and $k \rightarrow -k$ for the next t_r iterations. Without mea-
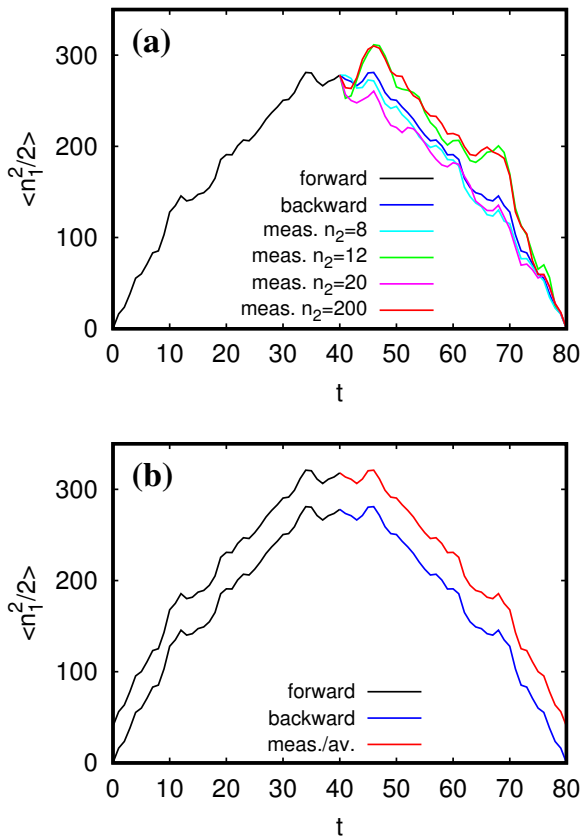
FIG. 1: Time dependence of the average energy of the first particle $E_1(t) = \langle n_1^2/2 \rangle$ for the initial state (6) with time evolution given by the quantum Chirikov standard map (2)-(3). The measurement of second particle and time reversal are performed after $t_r = 40$ quantum map (3) iterations. The black curves in both panels show the forward time evolution for $0 \leq t \leq t_r$; the blue curves show the backward time evolution $t_r \leq t \leq 2t_r = 80$ with the exact time reversal without measurement (using $T = 4\pi - \epsilon$). In panel (a) the curves of other colors show the backward time evolution after measurement of the second particle at momentum states $n_2 = 8$ (cyan), 12 (green), 20 (magenta), 200 (red). In panel (b) the red curve shows the backward time evolution after the second particle measurement detection at n_2 and averaging over all possible measurement results of n_2 values (black and red curves are shifted up by 50 units for a better visibility; red and blue curves coincide within numerical round-off errors ($\sim 10^{-13}$)). The system parameters are: $N = 1024$, $N_H = N^2$ and $\hbar_{\mathrm{eff}} = \epsilon = 5/8$, $K_{\mathrm{eff}} = 5$, $k = K_{\mathrm{eff}}/\hbar_{\mathrm{eff}} = 8$, $T = 4\pi \pm \epsilon$. We have verified that a further increase of N to values of 2048 and 4096 provide identical results up to numerical round-off errors (provided the free propagation eigenphases are properly computed as explained in the text at the beginning of this section).

surement the EPR wavefunction of two particles returns exactly to its initial state due to exact time reversibility of the quantum evolution. Also, in absence of entanglement of particles the measurement of the second particle does not affect the reversibility of the first particle which would exactly return to its initial state. However, in presence of entanglement the measurement of the second particle affects the time reversibility of the first particle in a nontrivial manner.

To illustrate the nontrivial features of measurements on time reversal of chaotic EPR pairs we use typical system parameters with $K = k\epsilon = k\hbar_{\mathrm{eff}} = 5$ and $k = 8$ (thus $\hbar_{\mathrm{eff}} = 5/8$). Such a value of $k = 8$ is not very high being well accessible to the present experimental facilities (see e.g. [25, 26, 32]).

In this first part to characterize the quantum time evolution we compute the one-particle probability (of the first particle) as: $w(n_1, t) = \sum_{n_2} |\psi(n_1, n_2, t)|^2$, (with the momentum wave function $\psi(n_1, n_2, t) = \langle n_1, n_2 | \psi(t) \rangle$), and the one-particle energy (of the first particle): $E_1(t) = \langle n_1^2/2 \rangle = \sum_{n_1} (n_1^2/2) \, w(n_1, t)$.

As initial state we take an entangled EPR pair without any symmetry and with more or less arbitrary coefficients at two momentum values:

$$\begin{aligned} |\psi(t=0)\rangle \;=\; & \Big(|0\rangle \otimes |0\rangle + 0.7|0\rangle \otimes |1\rangle + \\ & 0.3|1\rangle \otimes |0\rangle - 2|1\rangle \otimes |1\rangle \Big)/\sqrt{5.58} \,, \end{aligned} \quad (6)$$

where $|n_1\rangle \otimes |n_2\rangle$ represents the momentum basis states. Thus initially both particles are distributed over momentum states at $n_{1,2}$ being 0 or 1.

This state can be rewritten in the Schmidt decomposition [33] as :

$$|\psi(t=0)\rangle = \sum_{i=1,2} \alpha_i |u_i\rangle \otimes |v_i\rangle \quad (7)$$

with

$$\begin{aligned} \alpha_1 \;&=\; 0.8973 \quad, \quad \alpha_2 = 0.4414, \\ |u_1\rangle \;&=\; 0.3440|0\rangle - 0.9390|1\rangle, \\ |u_2\rangle \;&=\; 0.9390|0\rangle + 0.3440|1\rangle, \\ |v_1\rangle \;&=\; 0.0294|0\rangle + 0.9996|1\rangle, \\ |v_2\rangle \;&=\; 0.9996|0\rangle - 0.0294|1\rangle, \end{aligned} \quad (8)$$

The entropy of entanglement of this initial state is:

$$S = -\sum_i \alpha_i^2 \log_2(\alpha_i^2) = 0.7114 \,. \quad (9)$$

The time evolution of energy of the first particle $E_1(t) = \langle n_1^2/2 \rangle$ is shown in Fig. 1. At short initial times $t \leq 12$ we have an approximately diffusive energy growth $E_1(t) \approx Dt/2 \approx 16t$ with the diffusion coefficient $D \approx k^2/2 \approx 32$. For times $12 < t \leq t_r = 40$ the energy growth continues but its rate decreases due to the quantum interference effects being similar to the Anderson localization [19, 21, 23]). After $t_r = 40$ iterations of forward propagation in time, the projective measurement is performed for the second particle and the evolution of
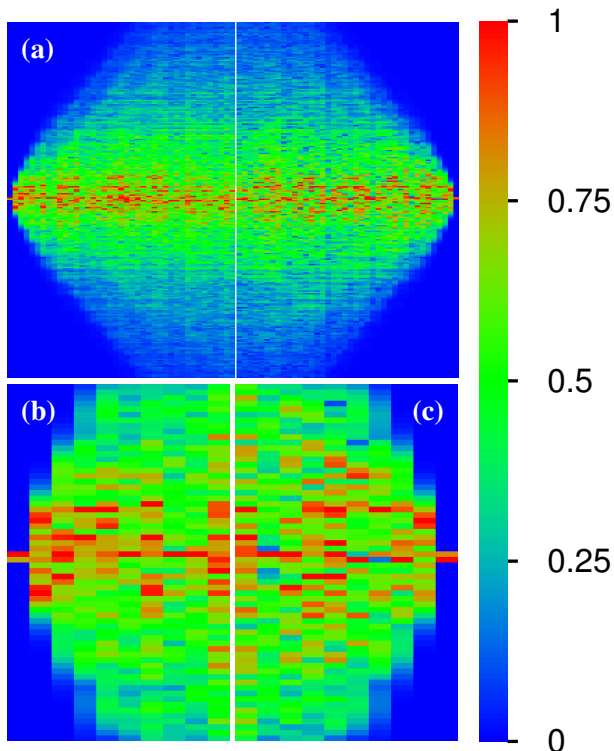
FIG. 2: Panel (a) shows the time evolution of probability of the first particle $w(n_1, t)$ (color density plot) for parameters of Fig. 1 and $-128 \leq n_1 < 128$ (y-axis), $0 \leq t \leq 80$ (x-axis), $t_r = 40$. The measurement and time reversal are done after t_r map (3) iterations with the second particle detected at the momentum value $n_2 = 12$. The thin white vertical line marks the time $t_r = 40$ of measurement and the beginning of backward iterations. The numbers of the color bar correspond to $[w(n_1, t)/w_{\max}(t)]^{1/4}$ with $w_{\max}(t) = \max_{n_1} w(n_1, t)$ being the density maximum at a given value of t. Panels (b) and (c) provide a zoom for $-32 \leq n_1 < 32$ (both panels) and $0 \leq t < 10$ (b) or $70 < t \leq 80$ (c).

FIG. 3: Same as Fig. 2 but for the second particle measured at $n_2 = 200$.

the first particle is reversed in time with a replacement $T = 4\pi + \epsilon \to 4\pi - \epsilon$ and $k \to -k$ (effective backward propagation in time).

In the top panel Fig. 1(a) we show the energy $E_1(t)$ dependence on time for forward $0 \leq t \leq t_r$ and backward evolution $t_r < t \leq 2t_r$ for different results of projective measurement, done after $t_r = 40$ iterations, giving (projecting) the second particle at different momentum states chosen as $n_2 = 8; 12; 20; 200$. For each measured n_2 value we have a different curve $E_1(t)$ of the time reversal or backward branch $t_r < t \leq 2t_r$ being different from the forward branch $0 \leq t \leq t_r$. However, all curves at different n_2 measured values have an energy decrease with time and approximately return to the initial energy value. Of course, in absence of measurements there is the exact time reversal of evolution and energy $E_1(t)$ is exactly symmetric with respect to the moment of time reversal and returns exactly to the initial value as it is
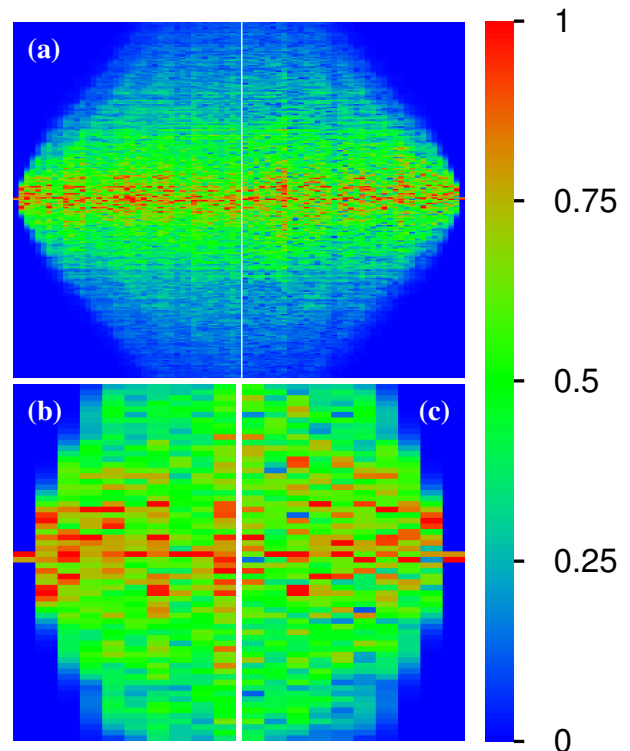
shown in Fig. 1(b) (blue curve). In the same panel we also present the result of backward evolution of $E_1(t)$ averaged over all projective measurements of second particle found at all possible momentum values n_2 (Fig. 1(b) red curve). The red and blue curves coincide up to numerical round-off errors being on a level of 10^{-13}. Such an exact coincidence of time reversal behavior without measurements and with averaging over all possible measurement results can be understood from the Feynman path integral formulation of quantum mechanics [35]. In this Feynman interpretation a specific projective measurement of second particle at n_2 value selects a specific entangled path of first particle which returns approximately to its initial state at $t = 0$.

Examples of the time evolution of the probability distribution of the first particle $w(n_1, t)$ are shown in Figs. 2, 3 for two cases of projective measurements of the second particle at momentum values $n_2 = 12, 200$ respectively (see also Appendix Fig. A.1). The measurement is done after $t_r = 40$ quantum map (3) iterations. For $0 \leq t \leq t_r$ the values of $w(n_1, t)$ are obtained by averaging the two-particle density over the second particle, after measurement of second particle $w(n_1, t)$ represents the probability distribution over momentum states of the remaining first particle. The results of Figs. 2, 3 show a diffusive type spreading of probability $w(n_1, t)$ during the time range $0 \leq t \leq t_r$. This corresponds to a diffusion

produced by the underlined classical chaotic dynamics (quantum corrections give a certain reduction of the diffusion rate as discussed above and in [19, 21]). After the projective measurement of the second particle and the time reversal of the propagation an inverse diffusion process takes place where the probability $w(n_1,t)$ returns approximately to the initial state of the first particle. This corresponds to a specific Feynman path selected by the projective measurement of the second particle immediately after the time t_r. Some snapshots of the probability distribution $w(n_1,t)$ corresponding to different results of measurements with different n_2 values are shown for specific time moments in Appendix Fig. A.2.
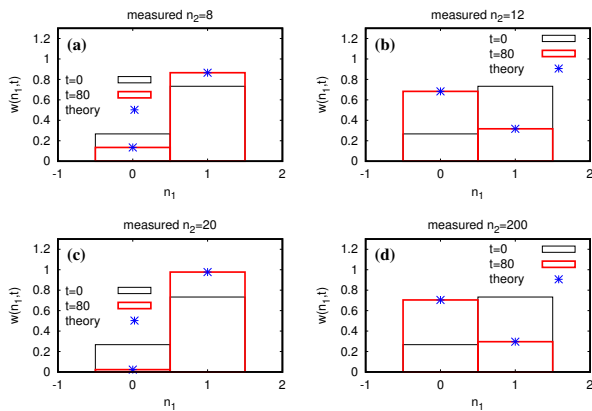
FIG. 4: Probabilities $w(n_1,t)$ of the first particle at initial time $t=0$ (black lines) and final time $t=2t_r=80$ (red lines) for the cases when the second particle is measured at $n_2=8$ (a), $n_2=12$ (b), $n_2=20$ (c) and $n_2=200$ (d) after the time reversal at $t_r=40$; system parameters are as in Fig. 1. The blue stars provide for each case the semi-analytical theoretical prediction for the final density at $t=2t_r=80$ obtained from the Schmidt decomposition (see text).

The probability distribution $w(n_1,t=2t_r)$ at the reversal time $t=2t_r$ is shown in Fig. 4. All probability is located at momentum states $n_1=0,1$ corresponding to the states populated by the first particle in its initial entangled state (6) (probability outside of these states is on a level of numerical round-off errors 10^{-13}). However, the values of the two return probabilities $w(n_1,t=2t_r)$ are affected by the measurement of the second particle and they are rather different from their values of the initial state (6).

The values of $w(n_1,t=2t_r)$ can also be computed from a "theoretical" state $|u_{\rm th}\rangle$ for the first particle obtained from the assumption that only the second particle is following the time evolution while the first particle remains fixed and measuring the second particle at $t=t_r$. The theoretical state is then given by $|u_{\rm th}\rangle = \alpha_1 C_1|u_1\rangle + \alpha_2 C_2|u_2\rangle$ where (for $j=1,2$) α_j and $|u_j\rangle$ are given by Eq. (8) used for the Schmidt decomposition of the initial state (7). The coefficients

C_j are obtained from the measurement procedure as $C_j = C_g \langle n_2|v_j(t_r)\rangle = C_g\, v_j(n_2,t_r)$ where $|v_j(t_r)\rangle$ are the second-particle states at the moment of measurement (after t_r iterations) and C_g is the global normalization constant of the theoretical state $|u_{\rm th}\rangle$. The blue stars in Fig. 4 show the values obtained from this theoretical state which coincide numerically (up to usual round-off errors) with the values of $w(n_1,t=2t_r)$ (also for the cases n_1 being different from 0 or 1 where are simple $w(n_1,t=2t_r)=0$).

The reason is that the Schmidt coefficients α_i remain unchanged during the forward propagation in time till the moment $t=t_r$ while the Schmidt vectors $u_1(n_1,t),v_1(n_2,t)$ and $u_2(n_1,t),v_2(n_2,t)$ evolve as one-particle wavefunctions computed numerically from (2) with the initial condition (7),(8). The measurement of the second particle, detected at momentum state n_2 at $t=t_r$, gives the above coefficients C_1 and C_2 and after the measurement the wavefunction of the first particle is: $\psi(n_1,t) = \alpha_1 C_1 u_1(n_1,t) + \alpha_2 C_2 u_2(n_1,t)$. During the backward evolution the components $u_1(n_1,t)$ and $u_2(n_1,t)$ return to their initial values providing exactly the theoretical state given above. Hence, the probability to find the first particle at $n_1=0$ is $w(n_1=0) = (0.3440\alpha_1 C_1 + 0.9390\alpha_2 C_2)^2$ and at $n_1=1$ it is $w(n_1=1) = (-0.9390\alpha_1 C_1 + 0.3440\alpha_2 C_2)^2$. As it is shown in Fig. 4 the results of this semi-analytical theory reproduce the numerically obtained probabilities (up to usual round-off errors).

IIIB. EPR pairs in kicked rotator at small $\hbar_{\rm eff}$ values

We also study the behavior of chaotic EPR pair in a deep semiclassical limit. For this we consider the quantum evolution on a torus of size N with $\epsilon=\hbar_{\rm eff}=2\pi/N$ and periodic conditions for the wavefunction in a momentum space $-\pi \leq p = \hbar_{\rm eff}n < \pi$. Such a time evolution of quantum maps on a quantum torus has been already studied in detail for the one-particle case (see e.g. [21, 36]). As above, we choose the effective chaos parameter $K_{\rm eff}=\hbar_{\rm eff}k=5$ such that the phase space of classical dynamics is mainly chaotic with only small integrable islands embedded in the chaotic component (the measure of these islands is approximately 2% [10]).

The initial state of the EPR pair is chosen as an entangled state given as the Schmidt decomposition of two pairs of coherent Gaussian states and with equal coefficients $\alpha_1=\alpha_2=1/\sqrt{2}$. More precisely, the initial components of the first particle are

$$|u_j(t=0)\rangle = |(x_0^{(j)},p_0^{(j)})_{\rm coh.}\rangle \qquad (10)$$
$$= C\sum_p \exp[-G(p-p_0^{(j)})^2 - ip\,x_0^{(j)}/\hbar_{\rm eff}]|p\rangle$$

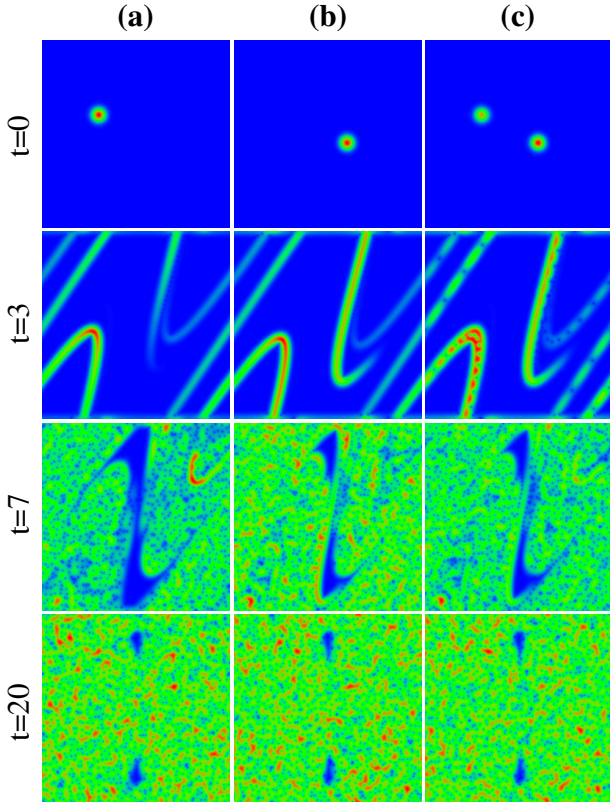with classical positions of the coherent wave packet at

FIG. 5: Density plots of Husimi functions of the first particle at certain time moments t. Columns (a) and (b) show the Husimi functions of the time dependent Schmidt components $|u_1(t)\rangle$ (a) and $|u_2(t)\rangle$ (b) of the first particle after $t = 0, 3, 7, 20$ iterations with the horizontal axis corresponding to $x_1 \in [0, 2\pi[$ and the vertical axis corresponding to $p_1 \in [-\pi, \pi[$ (or $n_1 \in [-N/2, N/2[$ with $p_1 = \hbar_{\text{eff}} n_1$ for $N = 2^{10}$). The initial conditions $|u_j(t = 0)\rangle$ (for $j = 1, 2$) are Gaussian coherent states (see (10) and text). The initial Schmidt components $|v_j(t = 0)\rangle$ of the second particle are also Gaussian coherent states of the same type with close positions (see text). Column (c) shows the Husimi functions of the first particle after the second particle being measured at $n_2 = 8$ after $t = t_r = 20$ iterations and followed by time reversal. The iteration times for the right column are $t_{(c)} = 40 - t$ with t being the time values shown in the figure for each row, i.e. $t_{(c)} = 40, 37, 33, 20$ (top to bottom). The color bar is the same as in Figs. 2 and 3 where the numbers correspond to $[H(x, p)/H_{\text{max}}]^{1/4}$ with $H(x, p)$ being the Husimi function of the first particle. System parameters are: $\epsilon = \hbar_{\text{eff}} = 2\pi/N = \pi \times 2^{-9}$, $K_{\text{eff}} = k\hbar_{\text{eff}} = 5$, $T = 4\pi \pm \epsilon$. The pixel resolution of each panel corresponds to $P \times P$ pixels with $P = 8\sqrt{N} = 2^8$.

$x_0^{(1)} = 0.3 \times (2\pi)$, $p_0^{(1)} = 0.1 \times (2\pi)$ and $x_0^{(2)} = 0.6 \times (2\pi)$, $p_0^{(2)} = -0.05 \times (2\pi)$. (Note that in (10) the p-sum runs over the values $p = 2\pi n/N$ with $n = 0, \ldots, N - 1$.) The parameter G is related to the width $\Delta p = \langle(\hat{p} - p_0^{(j)})^2\rangle^{1/2}$ of the wave packet in momentum space by $G = 1/(4\Delta p^2)$ and C is the normalization constant. Here we choose
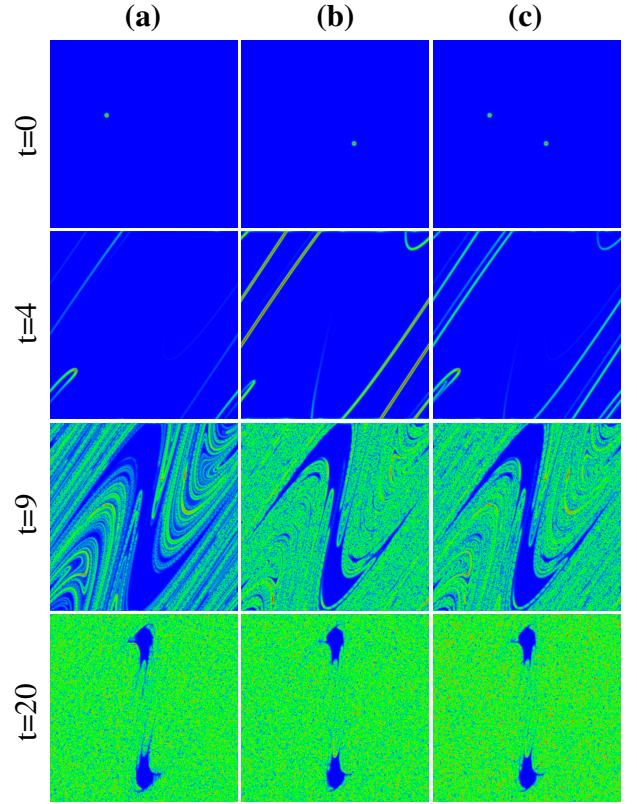
FIG. 6: Same as Fig. 5 but for $N = 2^{14}$ and modified iterations times $t = 0, 4, 9, 20$ (a), (b) or $t_{(c)} = 40 - t = 40, 36, 31, 20$ (c) (top to bottom); $\epsilon = \hbar_{\text{eff}} = 2\pi/N = \pi \times 2^{-13}$, $K_{\text{eff}} = k\hbar_{\text{eff}} = 5$. The number of pixels per direction is $P = 8\sqrt{N} = 2^{10}$.

$G = 1/(2\hbar_{\text{eff}}) = N/(4\pi)$ such that $\Delta p = \sqrt{\pi/N}$ and $\Delta x = \hbar_{\text{eff}}/(2\Delta p) = \sqrt{\pi/N}$ are identical (note that here for both variables x and p the system size is 2π).

The initial Schmidt components $|u_j(t = 0)\rangle$ of the second particle are also Gaussian coherent states of the same type (10) with close initial positions $|v_j(t = 0)\rangle = |(x_0^{(j)} + \delta x, p_0^{(j)} + \delta p)_{\text{coh.}}\rangle$ shifted by $\delta x = \delta p = 2\pi/\sqrt{N} = 2\sqrt{\pi}\Delta p$.

We describe the probability distribution of the first particle components (10) in the phase space (x_1, p_1) by the Husimi function defined as $H(x, p) = |\langle(x, p)_{\text{coh.}}|u\rangle|^2$ where $|u\rangle$ is the first-particle state for which the Husimi function is computed and $|(x, p)_{\text{coh.}}\rangle$ is the coherent state (10) with the above choice of $G = 1/(2\hbar_{\text{eff}})$ at classical positions (x, p). The Husimi function corresponds to a smoothing of the Wigner function over the above values of Δx, Δp with $\Delta x \Delta p = \hbar_{\text{eff}}/2$ (see e.g. [36, 37] for a description of Husimi functions). We have numerically computed the Husimi function using an efficient algorithm based on FFT and for a grid size $(\delta x/8) \times (\delta p/8)$ (with the above values of δx and δp).

The Husimi functions of the first particle Schmidt com-

ponents u_1, u_2 are shown in Fig. 5 at different iteration times $t = 0, 3, 7, 20$ (in columns (a) and (b)) for $\hbar_{\text{eff}} = 2\pi/N$ and $N = 1024$. We see that due to the underlying classical chaos the initial coherent state spreads very rapidly over the whole available phase space, except the domain of integrable islands which can be occupied only after very long tunneling times. In column (c) of Fig. 5 we show the backward time evolution of the first particle wave packet obtained from the measurement of the second particle at the momentum state $n_2 = 8$ performed after $t_r = 20$ quantum map (3) iterations. We see that the backward evolution of the first particle has different Husimi distributions at different return time moments. However, at $t = 2t_r = 40$ the first particle returns to its initial coherent states of Schmidt components at $t = 0$ but with different weights. In Fig. 6 we show also a similar time evolution with measurement and time reversal for the smaller value $\hbar_{\text{eff}} = 2\pi/N$, $N = 10^{14}$ and the measured state $n_2 = 8$. As in Fig. 5 there is an exponentially rapid spreading of initial coherent wave packets which after measurement returns to the initial two coherent states but with different weights.
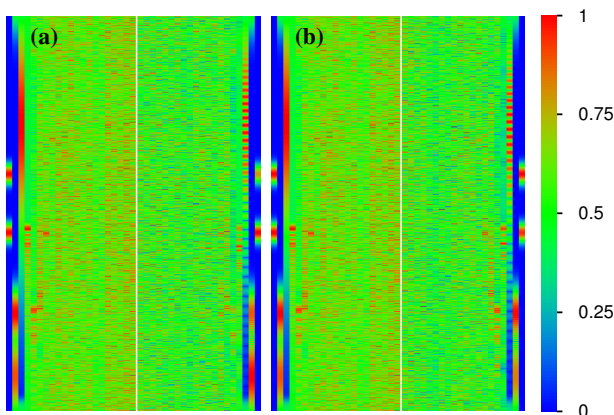
moment $t = 2t_r$ we still have two coherent wave packets for first particle which have the same shape as at the initial state but with different coefficients.

We also show the initial $t = 0$ and final $t = 2t_r = 40$ probability distributions of the first particle in Fig. 8 for different results of measurements of the second particle detected at $n_2 = 8, 12, 20, 200$. The weights of each coherent state at $t = 2t_r$ are determined from the Schmidt components of a theoretical state constructed in the same way as in the case of Fig. 4. The density of the theoretical state coincides with the final density at $t = 2t_r$ up to usual numerical round-off errors (only the maximum of each theoretical state is shown in Fig. 8 by a blue star).

Similar to the case of Fig. 7 with measured $n_2 = 8$ we show the time evolution $w(n_1, t)$ for other measured values $n_2 = 12, 20$ in Appendix Fig. A.3. For comparison we show in Appendix Fig. A.4 also the case of exact time reversal without measurements (i.e. with average over all measured n_2 values): here the distribution $w(n_1, t)$ is exactly symmetric with respect to time reversal at the moment $t = t_r = 20$.

FIG. 7: Panels show color density plot of $w(n_1, t)$ for the first particle time evolution and parameters of Fig. 5 with $-512 \leq n_1 < 512$ (y-axis) and $0 \leq t \leq 40$ (x-axis). The time values for $t \leq t_r = 20$ correspond to the exact forward iteration and for backward iterations $t_r < t \leq 2t_r = 40$, the measurement, done after t_r iterations, detects the second particle at $n_2 = 8$ (a) or $n_2 = 200$ (b). The thin vertical white line marks the time position of measurement $t_r = 20$ and the beginning of the time reversal backward iterations. The color bar has the same meaning as in Fig. 2.
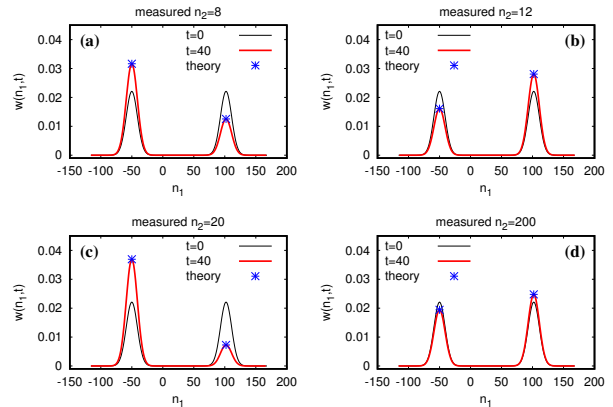

FIG. 8: Densities $w(n_1, t)$ of the first particle for the case of Fig. 5 are shown at initial $t = 0$ (black curves) and final $t = 2t_r = 40$ (red curves) time moments; the second particle is measured at $n_2 = 8$ (a), $n_2 = 12$ (b), $n_2 = 20$ (c) and $n_2 = 200$ (d). The blue stars provide for each case the maximum values of the density of the theoretical state obtained from the Schmidt decomposition (see text) and predicting the final density at $t = 40$. The theoretical density curves are identical to the red curves within numerical precision $\sim 10^{-13}$ but only their values at the two maximum positions are shown for a better visibility.

In Fig. 7 we show the time evolution of probability distribution $w(n_1, t)$ of first particle over momentum states n_1. For $0 \leq t \leq t_r$ this probability is averaged ob the second particle. As in Fig. 5 the projective measurement is done after $t_r = 20$ quantum map (3) iterations with the second particle detected at $n_2 = 8$. We see that the backward probability distribution $w(n_1, t)$ at $t > t_r$ is different from the forward one. However, at the return

IIIC. EPR pairs of cold atoms in a kicked optical lattice

Above we studied the properties of measurements and time reversal of EPR pairs in the regime of kicked rotator when the evolution takes place on a ring of size 2π.

However, the experiments with cold atoms in a kicked optical lattice [25, 26, 32] correspond to the situation when an EPR pair propagates on the infinite x axis containing many periods of size 2π. Due to the periodicity of potential the wavefunction of each particle is characterized by a quasimomentum with irrational values β (with $p = n + \beta$) that reduce the probability of the single atom time reversal as discussed in detail in [31]. Thus to model this experimental setup we consider the EPR propagation on an x interval of size $2\pi L$ containing L periods 2π of the optical lattice. We use periodic boundary conditions in x but during the time evolution the wave packet is not reaching the boundaries such that the boundary conditions are not important. In this case the free propagation of a particle between kicks is given by the same unitary operator as in (2) but now in numerical simulations the momentum takes discrete values $p = m/L$ with integers $m = -N/2, \ldots, N/2 - 1$ and $N = LN_r$ where L gives the number of different quasimomentum values β and N_r gives the number of integer values of momentum p. The integer p values corresponds to the rotator case. The kick operator remains the same as in (2) but the position operator now takes the discrete values $x = 2\pi m L/N$ (m having the same integer values as above) corresponding to the interval $[-\pi L, \pi L[$. As in the previous Sections the numerical simulations are done with the propagation of the full wavefunction using its Schmidt components. This allows to reach very high N and L values required to eliminate boundary effects. As it was shown in previous Sections this computational method gives the same results as the full wavefunction propagation with 2D FFT (up to numerical precision). We use as maximal values $N = 2^{22}$ with $L = 2^{14}$, $N_r = 2^8$.

Below we present results for time reversal for chaotic EPR pair in a kicked optical lattice. The momentum and energies are measured in recoil units as described in [31] that corresponds to dimensionless units of p used above. As in the last subsection the initial state is given an entangled state given as the Schmidt decomposition of two pairs of coherent Gaussian states and with equal coefficients $\alpha_1 = \alpha_2 = 1/\sqrt{2}$. However, now the parameter G in (10) is given by $G = 1/(4\Delta p)^2$ with $\Delta p = 0.01$ and due to notational reasons the parameter h_{eff} in (10) is replaced with unity (not to be confused with $h_{\text{eff}} = 5/8$ mentioned below). The corresponding width of the Gaussian packet in position representation is $\Delta x = 1/(2\Delta p) = 50 \approx 8 \times 2\pi$ corresponding roughly to 8 periods of the optical lattice. The center and phase parameters of (10) of the two Schmidt components for the first particle are $p_0^{(1)} = 1$, $p_0^{(2)} = 2$, $x_0^{(1)} = \pi$ (in the middle of the cell of index $m = 0$) and $x_0^{(2)} = 3\pi$ (in the middle of the cell of index $m = 1$). The values for the two corresponding Schmidt components of the second particle are $p_0^{(1)} = -1$, $p_0^{(2)} = -2$, $x_0^{(1)} = \pi$ and $x_0^{(2)} = 3\pi$, i.e. negative $p_0^{(j)}$ values and same $x_0^{(j)}$ values with respect to
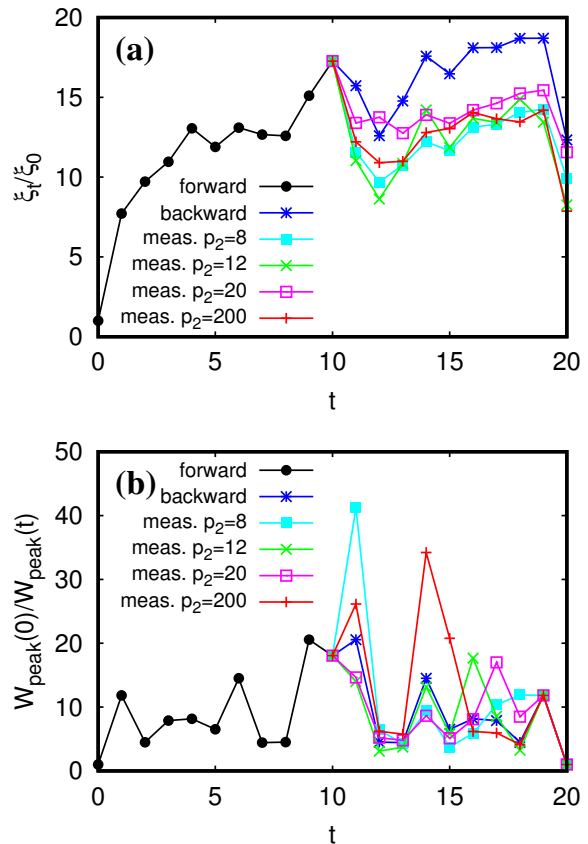

FIG. 9: Time dependence of rescaled IPR ξ_t/ξ_0 (a) and peak probability (b) of first particle for a chaotic EPR pair in a kicked optical lattice: the time forward evolution is marked by black points; full backward evolution is marked by blue stars (time reversal is done at $t = t_r = 10$ without measurement), backward evolution with measurement of the moment p_2 of the second particle done at t_r is shown by different color symbols for different measured p_2 values with $p_2 = 8$ (cyan full squares), $p_2 = 12$ (green crosses), $p_2 = 20$ (magenta open squares), $p_2 = 200$ (red pluses). System parameters are $\hbar_{\text{eff}} = \epsilon = 5/8$, $K_{\text{eff}} = 5$, $k = K_{\text{eff}}/\hbar_{\text{eff}} = 8$, $T = 4\pi \pm \epsilon$ (as in Fig. 1) and $N = LN_r = 2^{22}$, $L = 2^{14}$, $N_r = 2^8$. The initial state of the EPR pair is described in the text.

the first particle.

Concerning the Chirikov map we use the same parameters of the first subsection IIIA, i.e.: $\hbar_{\text{eff}} = \epsilon = 5/8$, $K_{\text{eff}} = 5$, $k = K_{\text{eff}}/\hbar_{\text{eff}} = 8$, $T = 4\pi \pm \epsilon$. The time reversal is done after $t_r = 10$ followed by a measurement of the second particle and the observation of first particle at the return moment $t = 2t_r = 20$.

As in [31] we characterize the quantum evolution of the first particle by the Inverse Participation Ratio (IPR) defined by $\xi_t = [\sum_{p_1} w(p_1, t)]^2 / \sum_p w^2(p_1, t) = 1/\sum_p w^2(p_1, t)$ where $w(p_1, t) = \sum_{p_2} |\langle p_1, p_2 | \psi(t) \rangle|^2$ are the probabilities of the first particle in the momentum space at time t and after summing over the second parti-
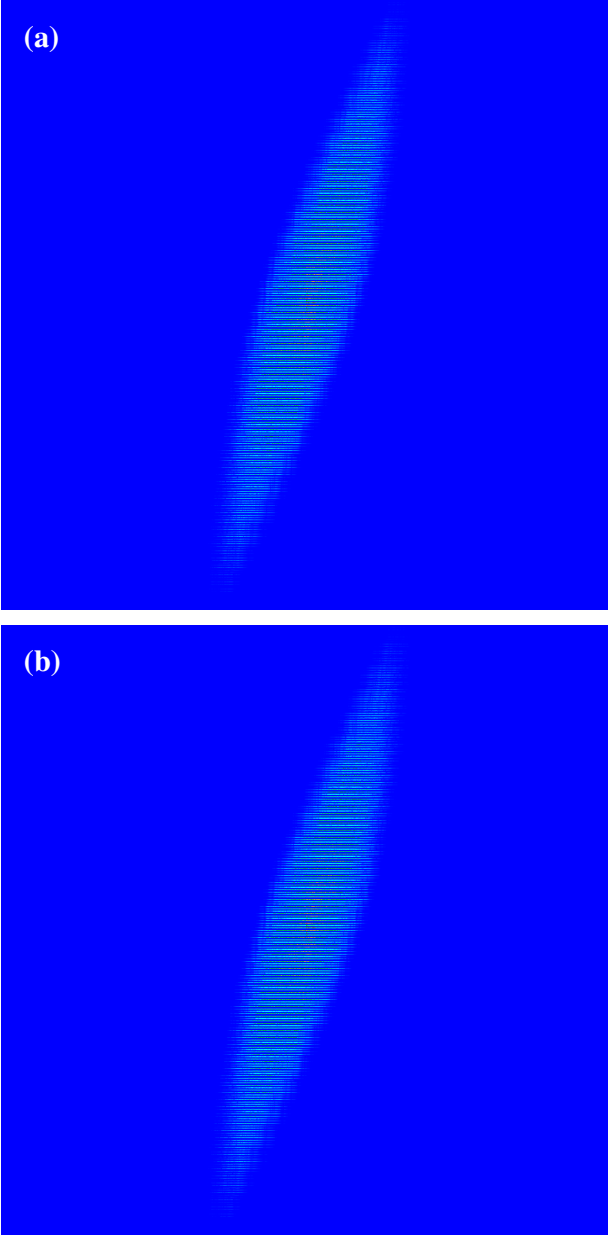
FIG. 10: (a) Husimi function of the first Schmidt component $|u_1(t)\rangle$ of the first particle at the return time $t = 2t_r = 20$ without measurement at time reversal $t = t_r = 10$; (b) Husimi function of the first particle at return time $t = 2t_r = 20$ with measurement of the second particle at $t = t_r = 10$ with detected momentum $p_2 = 12$. Parameters and initial state are as in Fig. 9. The color bar is the same as in Figs. 2 and 3 where the numbers correspond to $[H(x,p)/H_{\max}]^{1/8}$. Furthermore, the contrast of the image files has been artificially enhanced to increase the visibility of the regions with non-vanishing values of the Husimi function. x-axis shows the coordinate interval $-L/2 \leq x_1/2\pi < L/2$ for $L = 10^{14}$; y-axis shows the momentum interval $-N_r/2 \leq p_1 < N_r/2$ with $N_r = 2^8$.

cle momentum p_2 (the second identity in the expression of ξ_t holds if the probabilities $w(p_1,t)$ are properly nor-

malized). In addition we also compute the time variation of the relative peak probability $W_{\text{peak}}(0)/W_{\text{peak}}(t)$ where $W_{\text{peak}}(t) = \sum_{j=1,2} w(p_0^{(j)}, t)$ is the sum of the probabilities at the two initial peak positions $p_0^{(j)} = j$ (with $j = 1, 2$) in momentum space.
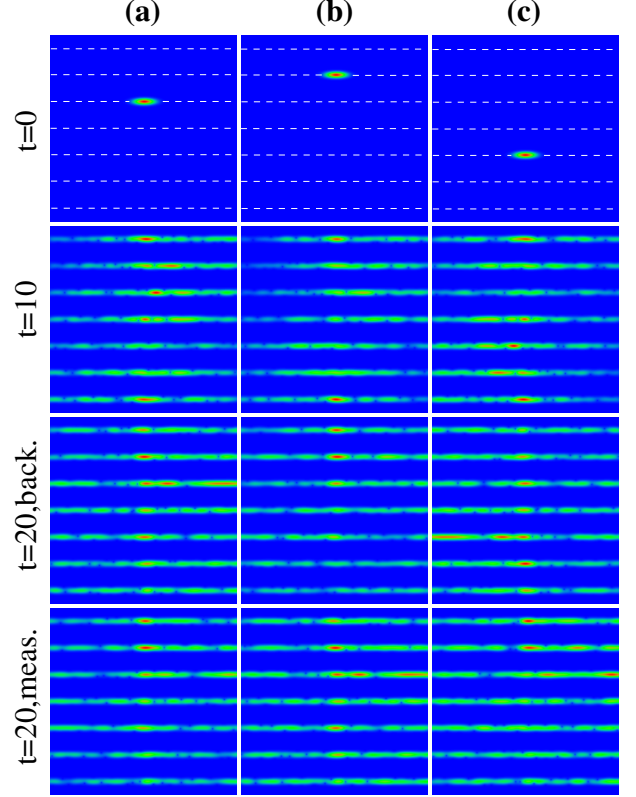

FIG. 11: Zoom of Husimi functions shown in the range $-3.5/256 \leq x_{1,2}/(2\pi L) \leq 3.5/256$ (corresponding to 448 periods of the optical lattice), $-3.5 \leq p_{1,2} \leq 3.5$; the top three rows show the Husimi functions of the Schmidt components $|u_1(t)\rangle$ (a), $|u_2(t)\rangle$ (b), $|v_1(t)\rangle$ (c) at $t = 0$ (1st row), $t = 10$ (2nd row) and the return time $t = 20$ for the case with no measurement (3rd row). The last row $t = 20, meas$ shows the Husimi functions of the first particle at the return time $t = 20$ with the measured momentum of the second particle at $t = 10$ being $p_2 = 8$ (a), $p_2 = 12$ (b), $p_2 = 20$ (c). The color bar is the same as in Figs. 2 and 3 where the numbers correspond to $[H(x,p)/H_{\max}]^{1/4}$. The dashed white horizontal lines in top row mark integer momentum values.

The time dependence of the relative IPR value ξ_t/ξ_0 is shown in Fig. 9(a). Up to the reversal time $t_r = 10$ we have an approximately diffusive growth of IPR $\xi_t/\xi_0 \propto \sqrt{t}$ corresponding to the energy diffusion well seen in Fig. 1. After the time reversal this growth is stopped but at the return time $t = 2t_r = 20$ there is no real return to the initial IPR value at $t = 0$. The reason is that the time reversal is exact only for quasimomentum values $\beta = 0$ (integer p values) and only approximate for rather small β close to zero or unity. This point is discussed

in detail in [31]. In fact the inversion of IPR is better for the case presented in [31] (see Fig.1 there) since the kick amplitude k is significantly smaller ($k = 4.5$ there vs. $k = 8$ here). The new feature well seen in Fig. 9(a) is that the measurement of the momentum of the second particle after $t = t_r = 10$ map iterations significantly affects the return behavior of IPR.

To demonstrate that certain characteristics have an exact return to the initial value (up to numerical precision) we show in Fig. 9(b) the time dependence of the probability ratio $W_{\text{peak}}(0)/W_{\text{peak}}(t)$. Due to conservation of quasimomentum β the probability $W_{\text{peak}}(t)$ is influenced only by the components of the wavefunction with $\beta = 0$ which have an exact time reversal and the final value $W_{\text{peak}}(t = 2t_r)$ is identical to its initial value $W_{\text{peak}}(0)$ (up to numerical precision). However, the measurement of the second particle at $t = t_r = 10$ affects the time evolution of $W_{\text{peak}}(0)/W_{\text{peak}}(t)$ at intermediate times $11 \leq t \leq 18$ as it is well seen in Fig. 9(b). Note that $W_{\text{peak}}(t)$ is given by the sum of probabilities over the two initial peak probabilities of the first particle at integer values of p. Due to that we have the exact return of $W_{\text{peak}}(t)$. However, at the return moment $t = 2t_r = 20$ the relative distribution of the return probability over the two initial peak positions is strongly affected by the measurement of the second particle as we show below.

We illustrate the global spreading of the initial wavefunction by showing the Husimi function in (x, p) plane in Fig. 10. The top panel shows the Husimi function of the first Schmidt component $v_1(p_1)$ at the return moment $t = 2t_r = 20$ (time reversal is done at $t_r = 10$ without measurement of second particle). In the bottom panel we show the Husimi function of the first particle at $t = 2t_r = 20$ for the case when a measurement detected the second particle at $p_2 = 12$ at $t_r = 10$. This figure shows that the main part of probability is not affected by time reversal and continues to spread in the phase space. Due to conservation of quasimomentum β the Husimi function is composed of narrow distributions (some kind of parallel lines) located at integer momentum values. This is a result of quasimomentum conservation and the narrow initial width $\Delta p = 0.01$ of the initial distribution in β at $t = 0$.

This line-type structure is better visible in the zoom of Fig. 10 shown in Fig. 11. Here we show time snapshots of the Husimi function of Schmidt components $|u_1(t)\rangle$, $|u_2(t)\rangle$ of the first particle and also $|v_1(t)\rangle$ of the second particle at $t = 0, 10, 20$ (from left to right columns and top to down rows). In the bottom row we show the Husimi function of the first particle at return time $t = 20$ with measured momentum of second particle being $p_2 = 8, 12, 20$ (left to right) at reversal time $t = t_r = 10$. Here we see a part of probability which returns to the initial distribution.

However, in global we see that the main fraction of the wave packet is not affected by time reversal. Indeed, as

it was shown in [31] only a relatively small fraction of the wave packet returns to the initial distribution (that was associated with the Loschmidt cooling). The reason is that the described procedure of time reversal is exact only for the quasimomentum value $\beta = 0$ and works approximately for other values $|\beta| \ll 1$ and $|\beta - 1| \ll 1$.
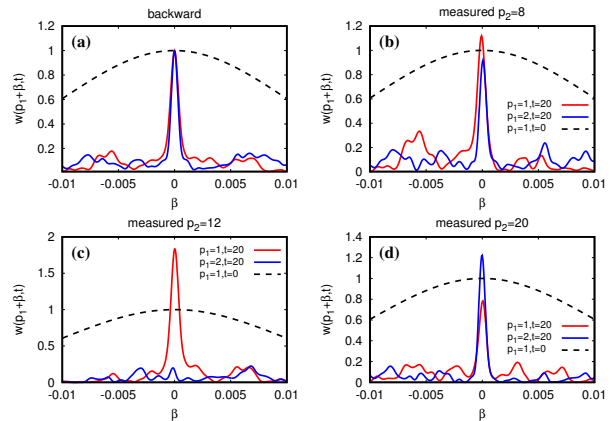

FIG. 12: Probability distribution $w(p_1 + \beta)$ of the first particle over quasimomentum β for two integer offsets $p_1 = 1$ or $p_1 = 2$; the initial Gaussian probability (of width $\Delta p = 0.01$) $t = 0$ is shown by the black dashed curve representing the first initial peak at $p_1 = 1$ (curve for the second initial peak at $p_1 = 2$ is identical). All shown distributions are rescaled by the maximum amplitude of the initial Gaussian distribution at $\beta = 0$. The rescaled probabilities at return the time $t = 2t_r = 20$ are shown by red and blue curves for the initial peaks at $p_1 = 1$ and $p_1 = 2$ respectively; the different panels correspond to: (a) time reversal at $t_r = 10$ without measurement; measurement at $t_r = 10$ detecting the second particle at $p_2 = 8$ (b), $p_2 = 12$ (c), $p_2 = 20$ (d). System parameters are as in Fig. 9.

To see in a better way the fraction of the wave packet returning to the initial distribution we show in Fig. 12 the probability distribution in quasimomentum β of the first particle at $t = 0$ and return time $t = 2t_r = 20$. In panel Fig. 12(a) the time reversal is done without measurement of second particle. The initial distribution has two peaks at $p_1 = 1, 2$ and the return probability exactly returns to its initial values at $\beta = 0$. However, the width of return distribution in β is significantly narrowed since the time reversal is only approximate for β different from (but close) zero. This effect, called Loschmidt cooling, is discussed in detail in [31]. The new feature present in Fig. 12 is that a measurement of the second particle at $t = t_r = 10$ significantly affects the peak probabilities at two initial positions $p_1 = 1, 2$ due to the entanglement of the EPR pair. At the same time the sum of probabilities of the two peaks at $p_1 = 1, 2$ remains exactly equal to the initial peak probability sum at $t = 0$ since the time reversal is exact for $\beta = 0$ (see also Fig. 9(b)). As for the above case of the kicked rotator, we interpret the fact that a measurement of second particle drastically affects
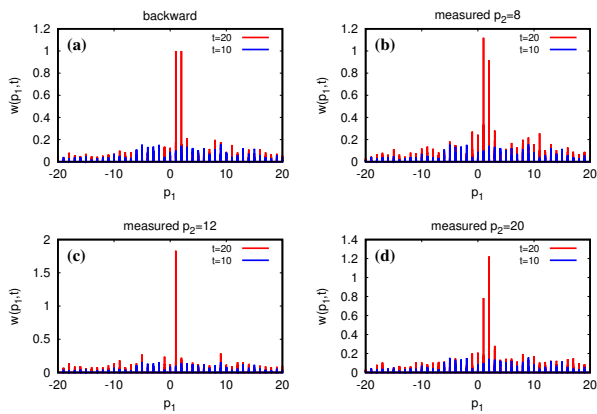
FIG. 13: Similar as in Fig. 12 but the results are shown on a larger momentum range of the first particle $-20 \leq p_1 \leq 20$; blue curves show the probability at the moment of time reversal $t = t_r = 10$, red curves show the probability at return time $t = 2t_r = 20$; the different panels correspond to the same cases of Fig. 12 (without or with measurement and detected p_2 values) and all densities are rescaled as in Fig. 12. The shown curves also integrate the data for non-integer values of p_1 but the density values at non-integer p_1 are essentially zero (in graphical precision).

the return path of the first particle with a specific Feynman path [35] selected by measurement of the entangled second particle at the moment of time reversal.

The distribution of probabilities of the first particle at times $t = t_r = 10$ and $t = 2t_r = 20$ is also shown in Fig. 13 on a larger scale of momentum p_1. We see that there is a broad background of probability of the first particle which diffusively spreads in momentum due to quantum chaos and which is not significantly affected by the time reversal. However, we also see that at the return time $t = 2t_r = 20$ there appear two very high peaks near momentum positions of the initial distribution. The amplitudes of these two peaks are strongly affected by a measurement of the second particle at time reversal $t_r = 10$. Even if the total probability in these two peaks at $t = 20$ is small compared to the total probability, their very high peak amplitudes allow to detect them in a very robust way. In fact, as it was shown in [38, 39] for reversal of acoustic waves, the chaotic dynamics allows to enhance the time reversal signal making it much more visible in presence of chaotic background. Here we have a similar situation that potentially allows to realize and detect the time reversal of entangled quantum cold atoms. The time reversal of cold atoms without measurement at the moment of time reversal has been realized in [32].

Here we presented results for measurements which detect a specific momentum value of second particle. Additional results for a measurement projection on a broader distribution of momentum p_2 with a certain width Δp_2 are presented in Appendix Fig. A.5, Fig. A.6. In this case

the time reversal also reproduces the the peaks of probability of first particle near their initial positions. These results show that a measurement device, which is modeled by a width Δp_2, affects the probability distribution of first particle at the return moment $t = 2t_r$.

Above we considered an initial entangled state with a narrow probability distribution near two integer momentum values of the EPR pair. We suppose that in an experimental setup initially ultra cold atoms can be trapped at very low temperatures corresponding to p values close to zero. Then a field pulse can move the momentum to higher p values being close to their integer values (in recoil units). The entanglement between the atoms can be created due to their initial interactions which is later switched off, e.g. with the help of the Feshbach resonance. It is also possible that both atoms have an initial momentum close to zero but being entangled they may have a certain spacial separation. Here we consider the case of distinguishable atoms that can be realized by taking two identical atoms but at different hyperfine states. Such a difference of internal atomic structure allows to measure one atom without affecting the other one. Of course, such type of experiments are very challenging but the technological progress allows now to perform operations with two entangled atoms (see e.g. [40]) and we expect that the experimental investigation of chaotic EPR pairs can be realized soon in cold atom experiments.

IV. DISCUSSION

In this work we analyzed the case when the evolution of an EPR pair is chaotic in the classical limit of small Planck constant. At the same time the system dynamics is reversible in time both in classical and quantum cases. In the classical case the errors grow exponentially with time due to dynamical chaos that breaks the time reversal of evolution is presence even of very small errors. In contrast the quantum evolution remains relatively stable to quantum errors due to the existence of instability only during a logarithmically short Ehrenfest time scale. Our main objective was to analyze how measurements of one particle of a chaotic and entangled EPR pair affects the time reversal of the remaining particle. We find that this particle retains an approximate time reversal returning to one of all configurations representing the initial entangled EPR state. We explain such an approximate time reversal on the basis of the Feynman path integral formulation of quantum mechanics according to which a measurement selects a specific configuration which returns to its initial state via time inverted specific pathway. We show that the Schmidt decomposition of the initially entangled EPR state allows to identify the final quantum state at the return time.

Here we considered the chaotic EPR pairs in the case of the quantum Chirikov standard map. This system has

been already realized in experiments with cold atoms in kicked optical lattices [25, 26]. Moreover, the time reversal, proposed in [31], has been realized experimentally by the Hoogerland group [32]. However, in this experiment the interplay aspects of entanglement and measurement for time reversal had not been studied. At present advanced cold atoms techniques allow to investigate various quantum correlations of entangled pairs of atoms (see e.g. [40]) and we expect that experimental investigations of the time reversal of chaotic EPR pairs, discussed here, are possible. It may also be interesting to consider the time reversal for two entangled Bose-Einstein condensates (BECs) with their chaotic evolution in a kicked optical lattice following the proposal of time reversal for a single BEC described in [41].

ACKNOWLEDGMENTS

APPENDIX

Here we present supplementary Appendix figures Figs. A.1 - A.6 referred in the main text.
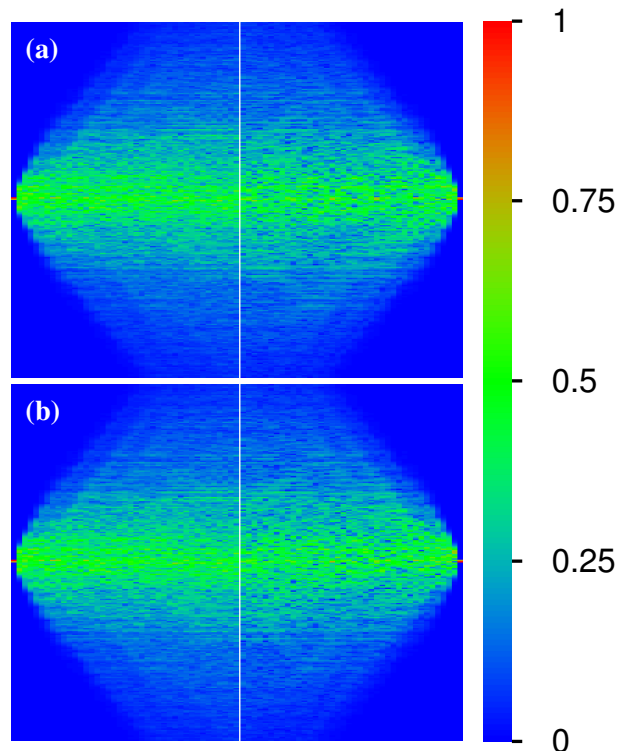
———————

FIG. A.1: Panel (a) is as panel (a) of Fig. 2 and panel (b) is as panel (a) of Fig. 3 but with densities renormalized by a global maximum such that the numbers of the color bar correspond to $[w(n_1,t)/w_{\mathrm{max,tot}}]^{1/4}$ with $w_{\mathrm{max,tot}} = \max_{(n_1,t)} w(n_1,t)$ being the global maximum with respect to all n_1 and t values.

[1] A. Einstein, B. Podolsky, and N. Rosen, *Can quantum-mechanical description of physical reality be complete?*, Phys. Rev. **47**, 777 (1935).

[2] E. Schödinger, *Die gegenwärtige situation in der quantenmechanik*, **23**, 807-812, 823-828, 844-849 (1935) [English translation J.D. Trimmer, *The present situation in quantum mechanics: a translation of Schrödinger's "cat paradox" paper*, Proc. Amer. Philos. Soc. **124**, 323-338 (1980)].

[3] M.A. Nielson, and I.L.Chuang, *Quantum computation and quantum information*, Cambridge University Press, Cambridge UK (2000).

[4] I. Bengtsson, and K. Zyczkowski, *Geometry of quantum states. An introduction to quantum entanglement*, Cambridge University Press, Cambridge UK (2017).

[5] I.H. Deutsch, *Harnessing the power of the second quantum revolution*, PRX Quantum **1**, 020101 (2020).

[6] M.D. Reid, P.D. Drummond, W.P. Bowen, E.G. Cavalcanti, P.K. Lam, H.A. Bachor, U.L. Andersen, and G. Leuchs, *Colloquium: The Einstein-Podolsky-Rosen paradox: from concepts to applications*, Rev. Mod. Phys. **81**, 1727 (2009).

[7] F. Haake, *Quantum signatures of chaos*, Springer, Berlin (2010).

[8] V. Arnold, and A. Avez, *Ergodic problems in classical mechanics*, Benjamin, NY (1968).

[9] I.P. Cornfeld, S.V. Fomin, and Y.G. Sinai, *Ergodic theory*, Springer-Verlag, Berlin (1982).

[10] B.V. Chirikov, *A universal instability of many-dimensional oscillator systems*, Phys. Rep. **52**, 263 (1979)

[11] A. Lichtenberg, and M. Lieberman, *Regular and chaotic dynamics*, Springer, New York, NY, USA (1992).

[12] L. Boltzmann, *Weitere Studien uber das Warmegleichgewicht unter Gasmolekulen*, Wiener Berichte **66**, 275 (1872).

[13] J.Loschmidt, *Uber den Zustand des Warmegleichgewichts eines Systems von Korpern mit Rucsicht auf die Schwerkraft*; II-73; Sitzungsberichte der Akademie der Wissenschaften, Wien, Austria, p. 128 (1876).

[14] L.Boltzmann, *Uber die Beziehung eines Allgemeine Mechanischen Satzes zum Zweiten Haupsatze der Warmetheorie*; II-75; Sitzungsberichte der Akademie der Wissenschaften: Wien, Austria, p. 67 (1877).

[15] J.E. Mayer, and M. Goeppert-Mayer, *Statistical mechanics*, Jon Wiley & Sons, N.Y. (1977).

[16] E. Schrödinger, *Uber die Umkehrung der Naturgesetze*, Sitzungsberichte der preussischen Akademie der Wissenschaften, physikalische mathematische Klasse, **8(9)**, 144 (1931).
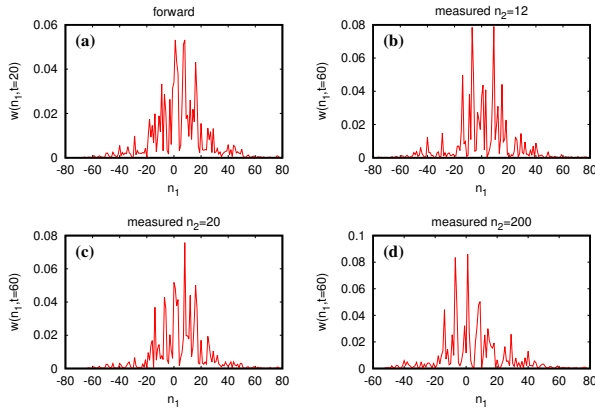
FIG. A.2: Densities $w(n_1, t)$ of first particle shown at $t = 20$ (a) (case of forward iteration) and three cases of backward iteration at $t = 60$ with the second particle being measured at $n_2 = 12$ (b), $n_2 = 20$ (c) or $n_2 = 200$ (d); system parameters are as in Fig. 1.
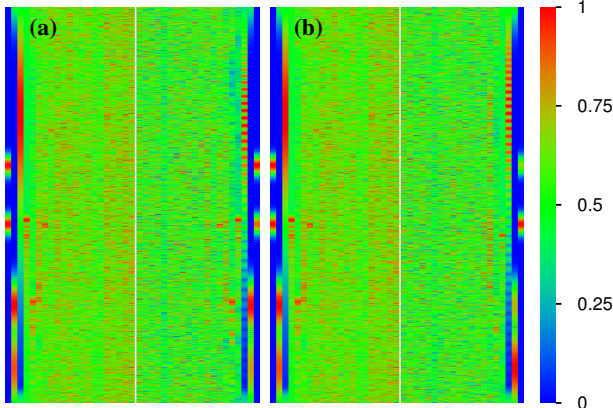

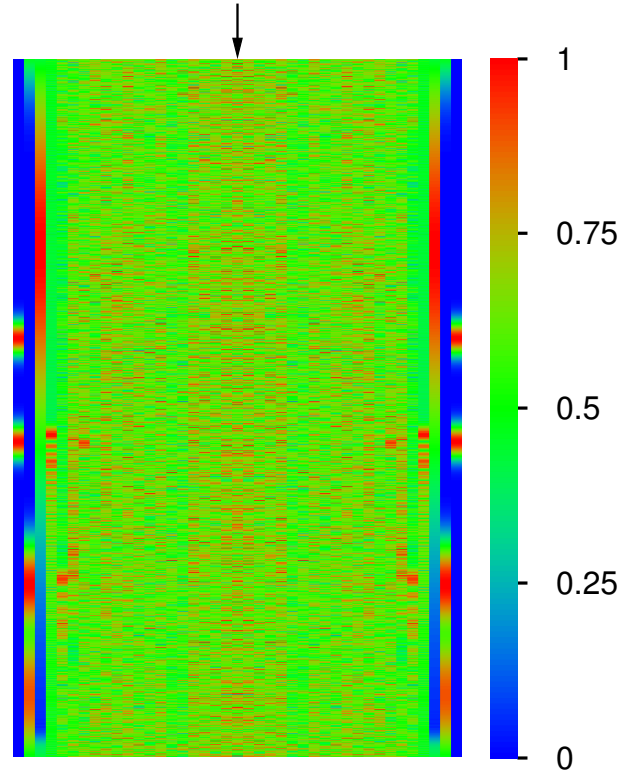FIG. A.3: Same as Fig. 7 but for the measured momentum $n_2 = 12$ (a) and $n_2 = 20$ (b).

FIG. A.4: Same as Fig. 7 but with the exact backward iteration for $t > t_r = 20$ without measurement (or averaged over all measured values of the second particle momentum n_2).

[17] R. Chetrite, P. Muratore-Ginanneschi, and K. Schwieger, *E. Schrödinger's 1931 paper "On the Reversal of the Laws of Nature" ["Uber die Umkehrung der Naturgesetze", Sitzungsberichte der preussischen Akademie der Wissenschaften, physikalische mathematische Klasse, 8 N9 144-153]*, arXiv:2105.12617[physics.hist-ph] (2021).

[18] A.N. Kolmogorov, *Zur Umkehrbarkeit der statistischen Naturgesetze*, Mathematische Annalen, **113**, 766 (1937).

[19] B.V. Chirikov, F.M. Izrailev, and D.L. Shepelyansky, *Dynamical stochasticity in classical and quantum mechanics*, Sov. Sci. Rev. **2C**, 209 (1981) [Sec. C-Math. Phys. Rev., Ed. S.P.Novikov, **2**, Harwood Acad. Publ., Chur, Switzerland (1981)].

[20] D.L. Shepelyanskii, *Dynamical stochasticity in nonlinear quantum systems*, Theor. Math. Phys. **49**, 925 (1981) [Teor. Mat. Fiz. **49**, 117 (1981) in Russian].

[21] B.V. Chirikov, F.M. Izrailev, and D.L. Shepelyansky, *Quantum chaos: localization vs. ergodicity*, Physica D **33**, 77 (1988).

[22] D. Shepelyansky, *Ehrenfest time and chaos*, Scholarpedia **15(9)**, 55031 (2020).

[23] D.L. Shepelyansky, *Some statistical properties of simple classically stochastic quantum systems*, Physica D **8**, 208 (1983).

[24] B. Chirikov, and D. Shepelyansky, *Chirikov standard map*, Scholarpedia **3(3)**, 3550 (2008).

[25] F.L. Moore, J.C. Robinson, C.F. Bharucha, B. Sundaram, and M.G. Raizen, *Atom optics realization of the quantum δ-kicked rotor*, Phys. Rev. Lett. **75**, 4598 (1995).

[26] J. Chabe, G. Lemarie, B. Gremaud, D. Delande, P. Szirftgiser, and J.C. Garreau, *Experimental observation of the Anderson metal-insulator transition with atomic matter waves*, Phys. Rev. Lett. **101**, 255702 (2008).

[27] P.W. Anderson, *Absence of diffusion in certain random lattices*, Phys. Rev. **109**, 1492 (1958).

[28] S. Fishman, D.R. Grempel, and R.E.Prange, *Chaos, quantum recurrences, and Anderson localization*, Phys. Rev. Lett. **49**, 509 (1982).

[29] S. Fishman, *Anderson localization and quantum chaos maps*, Scholarpedia **5(8)**, 9816 (2010).

[30] D.L. Shepelyansky, *Localization of diffusive excitation in multi-level systems*, Physica D **28**, 103 (1987).

[31] J.Martin, B.Georgeot, and D.L.Shepelyansky, *Cooling by time reversal of atomic matter waves*, Phys. Rev. Lett. v.100, p.044106 (2008).

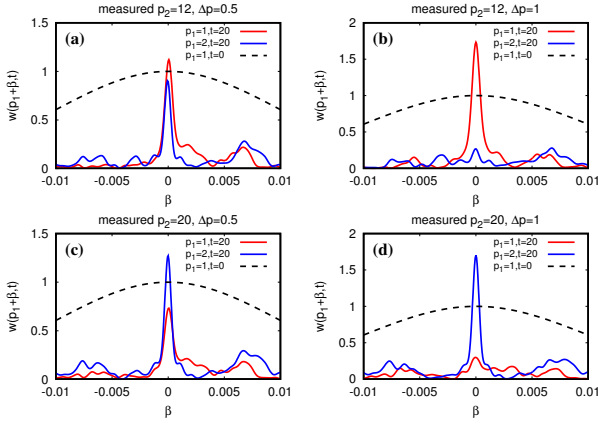[32] A. Ullah, and M.D. Hoogerland, *Experimental observation of Loschmidt time reversal of a quantum chaotic sys-*

FIG. A.5: Same as in Fig. 12 but the measurement projects the second particle on a Gaussian packet of width Δp_2 centered at $p_2 = 12$ (panel (a) with $\Delta p_2 = 0.5$ and panel (b) with $\Delta p_2 = 1$) and at $p_2 = 20$ (panel (c) with $\Delta p_2 = 0.5$ and panel (d) with $\Delta p_2 = 1$). The phase parameter of the Gaussian packet is $x_0 = 0$ for all cases.
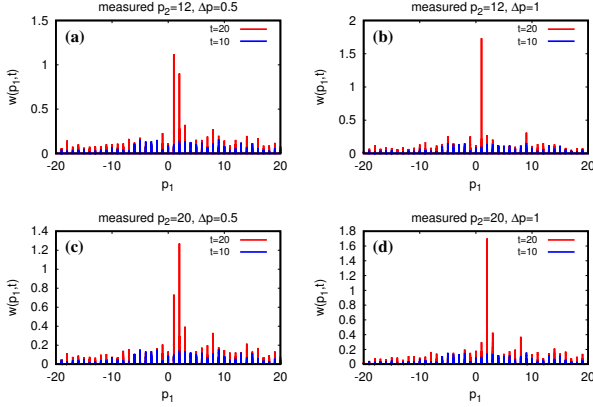

FIG. A.6: Same as in Fig. 13 for the cases of Fig. A.5 with a measurement projecting the second particle on a Gaussian packet (for different values of center and width).

tem, Phys. Rev. E **83**, 046218 (2011).

[33] E Schmidt, *Zur Theorie der linearen und nicht-linearen lntegralgleichungen*, Math. Ann. **63**, 433 (1907); English translation: G.W. Stewart, *FREDHOLM, HILBERT, SCHMIDT: Three Fundamental Papers on Integral Equations Translated with commentary by G.W.Stewart*, Available: http://www.umiacs.umd.edu/∼stewart/FHS.pdf (Retrieved January 2021).

[34] M.V. Fedorov, and N.I. Miklin, *Schmidt modes and entanglement*, Contemporary Physics **55(2)**, 94 (2014).

[35] R.P. Feynman, *Space-time approach to non-relativistic quantum mechanics*, Rev. Mod. Phys. **20(2)**, 367 (1948).

[36] K.M. Frahm, R. Fleckinger, and D.L.Shepelyansky, *Quantum chaos and random matrix theory for fidelity decay in quantum computations with static imperfections*, Eur. Phys. J. D **29**, 139 (2004).

[37] S.-J. Chang and K.-J. Shi, *Evolution and exact eigenstates of a resonant quantum system*, Phys. Rev. A **34**, 7 (1986).

[38] A. Derode, P. Roux, and M. Fink, *Robust acoustic time reversal with high-order multiple scattering*, Phys. Rev. Lett. **75**, 4206 (1995).

[39] J. de Rosny, A. Tourin, and M. Fink. *Coherent backscattering of an elastic wave in a chaotic cavity*, Phys. Rev. Lett. **84**, 1693 (2000).

[40] F. Borselli, M. Maiwoger, T. Zhang, P. Haslinger, V. Mukherjee, A. Negretti, S. Montangero, T. Calarco, I. Mazets, M. Bonneau, and J. Schmiedmayer, *Two-particle interference with double twin-atom beams*, Phys. Rev. Lett. **126**, 083603 (2021).

[41] J. Martin, B. Georgeot, and D.L. Shepelyansky, *Time reversal of Bose-Einstein condensates*, Phys. Rev. Lett. **101**, 074102 (2008).